The Research Council of Norway (NFR)

NORSAR

NORSAR Scientific Report No. 2-93/94

Semiannual Technical Summary

1 October 1993 – 31 March 1994

Kjeller, May 1994

APPROVED FOR PUBLIC RELEASE, DISTRIBUTION UNLIMITED

7 Summary of Technical Reports / Papers Published

7.1 A system for continuous global seismic threshold monitoring

Summary

Continuous threshold monitoring is a technique for using a seismic network to monitor a geographical area continuously in time. The method provides, at a given confidence level, a continuous assessment of the upper magnitude limit of possible seismic events that might have occurred in the target area. Three approaches are discussed in this paper.

Site-specific threshold monitoring: By 'focusing' a seismic network on a specific target site, continuous threshold monitoring of that site is achieved. We optimize the monitoring capability by tuning the frequency filters and array beams to known characteristics from previously recorded events at the site. We define the *threshold trace* for the network as the continuous time trace of computed upper magnitude limits of seismic events in the target area, at a 90 per cent confidence level.

Regional threshold monitoring: This involves conducting site-specific monitoring of a dense grid of geographical aiming points and requires the development of generic phase attenuation relationships for covering a specific geographical region. The regional threshold monitoring approach lends itself to illustration in the form of maps with color contour displays.

Global threshold monitoring: This is a natural extension of the regional monitoring approach, but requires a somewhat different strategy for effective implementation. Using a global network, and taking into account that phase propagation time is up to several tens of minutes, it is necessary to establish elaborate travel-time and attenuation tables, and to use a much coarser geographical grid than in the regional approach.

The regional and global threshold maps have advantages over standard network capability maps in being more accurate during time intervals when interfering seismic events occur. They can also more easily reflect special conditions such a particularly favorable source-station propagation paths, and have the advantage of not being tied to specific event detection criteria.

As discussed by Ringdal and Kværna (1992), continuous threshold monitoring offers a valuable supplement to traditional seismic techniques used in nuclear test ban monitoring. The method may also be useful for monitoring earthquake activity at low magnitudes for sites of special interest, as well as for monitoring earthquake aftershock sequences.

In this paper, an overview is given of the underlying principles for continuous threshold monitoring, together with a status report for the development of a prototype system for continuous seismic threshold monitoring on a global scale.

Introduction

Traditionally, seismic monitoring of earthquakes and underground explosions has relied upon applying signal detectors to individual stations within a monitoring network, associating detected phases and locating possible events in the region of interest. It is implicitly understood that such a network will have a detection threshold that varies with time. However, with methods being used in practical operation today, no attempt is made to specify this threshold as a function of time. During time periods when the background noise level is abnormally high, the event detection capabilities of such a network may be severely degraded. It is important to retain such information along with the information on the detected events.

In practice, the event detection procedure is often supplemented by assessments of network capabilities for the target region using statistical models for the noise and signal distributions. These models include station corrections for signal attenuation and a combinational procedure to determine the detection threshold as a function of the number of phase detections required for reliable location (Sykes & Evernden 1982; Harjes, 1984; Hannon 1985; Ringdal 1986; Sereno & Bratt, 1989).

The noise models used in these capability assessments are not able to accommodate the effect of interfering signals, such as the coda of large earthquakes, which may cause the estimated thresholds to be quite unrealistic at times. Furthermore, only a statistical capability assessment is achieved, and no indication is given as to particular time intervals when the possibility of undetected seismic events is particularly high.

Another shortcoming of traditional signal detection-based monitoring is their inability to provide upper bounds on magnitudes of non-detected seismic events. This could be important, e.g., if a teleseismic network fails to detect an event that is known to have occurred (for example, through local network recordings). Even more important, it would be useful for discrimination purposes to obtain a network-based upper limit on M_S for a given seismic event for which no surface waves are detected. Again, traditional methods do not provide such "negative evidence".

The continuous threshold monitoring technique has been developed to address these problems. The basic principles were described by Ringdal & Kværna (1989), who showed that this method could be useful as a supplement to event detection analysis. In this paper we expand further on the utility of this method, with particular emphasis on seismic threshold monitoring on a global scale, using a global network. Some examples are given on how such monitoring could be achieved in a practical prototype system, which might be suitable at an International Data Center for monitoring a Comprehensive Test Ban Treaty (CTBT).

General approach

The basic idea behind the threshold monitoring method is, for any given point in time, to assess the largest magnitude of events in a given target region that might go undetected by

a monitoring network. These magnitude estimates are computed by combining observations of the amplitude of the seismic data at different arrays and/or single stations.

For computation of site-specific continuous magnitude thresholds the following procedure is required (for details, see Ringdal & Kværna, 1992):

- For each location-station-phase combination, estimate continuously the seismic amplitude levels. If the station is an array, we use short-term averages (STAs) of filtered beams to represent the amplitude levels. The steering parameters of the beams will then correspond to the apparent velocity and azimuth of the actual phase. The filter bands are chosen such that good signal-to-noise ratio (SNR) is ensured. If the observation unit is a three- or single-component station, the STA values are computed from a filtered single channel.
- When considering a potential event at a given time and location, measure the seismic amplitude levels at the expected arrival times for the relevant seismic phases. The travel times for each phase can be taken from standard travel time tables, or by processing events with known location and origin time.
- In order to relate the STA observations to actual magnitude estimates, apply the formula

$$m = \log(STA) + b(\Delta, h) \quad (1)$$

  where m is the estimated magnitude, STA is the representation of the seismic amplitude level and b is a distance-depth correction factor for each location-station-phase combination. The correction factors can be obtained by processing events with known magnitudes, or by using standard attenuation values.
- For assessing the significance of these magnitude estimates, assume that they are sampled from a normal distribution with a given standard deviation. Experience with signal amplitude variation across the NORSAR array indicates that a standard deviation of 0.2 is a good value for a small epicentral area.
- The magnitude limits computed by this algorithm are tied to a given confidence level, initially set to 0.9. This means that the estimated limits represent the largest magnitude of a possible hidden event, in the sense that there is at least a 90 per cent probability that one or more of the observed amplitude values would be exceeded by the signals from an event with magnitude above these limits.

Global threshold monitoring -- basic principles

In principle, global threshold monitoring can be achieved by conducting site-specific monitoring of a grid of target points covering the globe. The density of the grid and the interpolation technique applied will determine the quality of the results.

We have adopted the method described by Vinje et al (1992) to develop global grid point systems. This method applies triangulation of an icosaeder to construct regularly sampled

wavefronts, and provides uniform geographical coverage of the globe at a specified grid density (Kværna, 1992).

Figs. 7.1.1 to 7.1.3 show three examples of such coverage, using 162, 642 and 2562 grid points, respectively. With the coarsest sampling (162 points) the circle corresponding to each grid point has a radius of 11.0 degrees. This radius is reduced to 5.5 and 2.75 degrees for the two denser grids, respectively.

The grid density to be used in practice is mainly a cost-performance trade-off. As described later in this paper, we have chosen the 642-point grid for the initial prototype of a global threshold monitoring system.

It is important to be aware that the density of the global TM grid is quite different from the beam deployment density for the arrays in the station network. For each array, a certain number of steering points will be selected (typically less than 100 for a small or medium aperture array, and several hundred for a large array). When calculating the threshold traces for a given TM grid point, the closest beam steering point is selected. Thus, there will be a potential beam steering loss that must be taken into account when calculating the "representative" threshold for the circle covered by the TM grid point.

The beam steering loss is mainly a function of array aperture and signal frequency. An illustration for the NORESS array is given in Figs. 7.1.4-7.1.5, showing 1 dB and 3 dB beam loss contours for P-type velocities (8 km/s and up). These loss contours are circles when shown in inverse velocity space, and the steering points therefore do not translate into equidistant geographical points. Thus, if mainly teleseismic distances are considered, the number of steering points for a given worst-case loss will be modest.

Calibration and time/azimuth tolerances

Ideally, global threshold monitoring requires access to magnitude calibration statistics for each target point and each station/phase combination considered. In a practical situation it will usually be impossible to obtain the necessary number of calibration events for each target point in the grid, and a different approach is therefore required.

Our approach is to develop a set of "generic" attenuation models. This can be done as a two-step process. The first step is to divide the earth into regions that are relatively homogeneous with respect to wave propagation characteristics. Within each region, an attenuation model is then established on the basis of available calibration data.

Using this approach, the distance-depth correction factors $b\,(\Delta, h)$ in (1) can be determined individually for each seismic phase, by applying a standard global attenuation model, in combination with region-specific station corrections.

In threshold monitoring there is a trade-off between the size of the target area and the tolerances of the parameter values used in the threshold computations. With a given grid, it is necessary to make the tolerances of each aiming point compatible with the grid spacing.

An illustration of the time and azimuth tolerances is given in Figs. 7.1.6 and 7.1.7. For example, if we increase the time windows over which we measure the signal levels, this has the effect of broadening the target area for the aiming point. At the same time, some of the resolution in the regional threshold variation will be lost. As shown in Fig. 7.1.6, the necessary time window corresponding to a typical teleseismic distance (see the highlighted area of Fig. 7.1.1) is of the order of ± 1 minute. A similar consideration applies to azimuth and slowness tolerances (see Fig. 7.1.7), and we refer to Kværna (1992) for details.

Implementation considerations

A convenient way to view the threshold monitoring system is to consider it as a set of objects and attributes.

The basic objects in threshold monitoring are the *Station* and the *GridPoint*. The *Network* is the collection of *Station* objects. The *Grid* is the collection of *GridPoint* objects.

A Station can be an array, a three-component station or a single-component station. The type of seismometer, digitizer, sampling rate and response function can vary, although for the TM purpose we will restrict ourselves to the short period processing band (typically 0.5 Hz and higher).

A GridPoint is an aiming point in geographical space. In site-specific monitoring, only one GridPoint is necessary, and the Grid consequently consists of only this one GridPoint.

In regional and global threshold monitoring, the Grid will consist of many GridPoints. The number of GridPoints and their density and distribution may vary according to the available Network, the monitoring requirements and the computing facilities available.

The Station object

The Station object has the following attributes:

a) Fixed attributes
   - Latitude, longitude, height
   - Types and deployments of sensors
   - System response
   - Sampling rate

b) Parameterized attributes
   - Number of beams
   - For each beam: Ux, Uy, beam configuration, filter band

The GridPoint object

The GridPoint object has the following attributes:

- Latitude, longitude, depth

For each station:

- A 0/1 indicator for P-phase
- A 0/1 indicator for S-phase
- Similar indicators for other phases used

For each nonzero Station-Phase combination:

- A filter band
- A pointer to the nearest beam
- A magnitude bias term

Threshold processing

For a given GridPoint, Origin Time, Station and Phase, an STA value is calculated as the maximum of N consecutive 2-second STA(1) values for the appropriate beam.

This STA value is converted to magnitude using an empirical conversion from STA to A/T, and then applying Veith-Clawson or other extended distance-depth corrections and adding/subtracting the appropriate GridPoint bias.

The set of magnitudes thus obtained is converted to a 90 percent threshold using the method of Ringdal & Kværna (1992).

Parameter selection

The beam deployment is made taking into account the need for regional characterization (for non-arrays as well as arrays) and the allowable worst-case beam loss for the appropriate regional coverage.

The beam configurations are set so as to obtain the optimum SNR for the actual beam in the frequency band used. The SNR is defined as the signal strength relative to the normal noise conditions (note that this is different from the optimum SNR for "coda phases").

The Grid is determined based upon the actual monitoring requirements and the resources available.

The filter bands are set for each GridPoint-Station-Phase combination and should be designed for optimum SNR for all events of interest in the area covered by the GridPoint.

Filter parameters

Initially, the prototype system will use a set of generic, wide-band filters.

We classify the distances into 4 ranges:

A: 0-10 degrees

B: 10-20 degrees

C: 20-90 degrees

D: 90-180 degrees

We classify the Stations as follows:

S1: Good HF propagation, low HF noise

S2: Stations with low LF noise, and which are not in the S1 category

S3: All other stations

We define the generic filter bands as follows:

F1: 0.5-2 Hz

F2: 1.5-6 Hz

F3: 2.5-10 Hz

F4: 4.0-16 Hz

The initial selection is as follows, for distance ranges A, B, C, D:

S1:	F4	F3	F2	F2
S2:	F3	F2	F1	F1
S3:	F3	F2	F2	F1

These filter bands should be refined on an individual station basis as experience accumulates.

STA calibration

Since STA values are used instead of A/T as a basis for magnitude estimates, it is necessary to introduce a conversion formula. From experiments with different short-period instrument types, we have found that such a relation can be well parameterized in the following way:

$$\log (A/T) = \log (STA \times cal) + c\,(resp, filter) \qquad (2)$$

where *cal* is the instrument calibration factor at 1 Hz, and *c* is a constant that is dependent on the instrument response and the filter band used to calculate the STA value. The constant *c* is derived empirically for each instrument and the filter band, as shown in Fig. 7.1.8.

Initial IDC implementation

The initial IDC implementation will comprise the following main features:

- Continuous global TM map
- 642 grid points
- 10 seconds update rate
- 7-day diskloop of STA values
- Site-specific traces extracted on request

It should be noted that the site-specific traces will be represented by the trace of the closest global grid point. "Optimum" site-specific traces may be available in the future.

It is currently envisaged that the following Threshold Monitoring services will be provided by the IDC:

- World threshold map (e.g., postcript file) at given point in time
- Site-specific trace (taken from world map) for specified target and time period
- Either data points or trace plot provided
- Specification of IDC events associated with peaks on the TM plot
- Use of CenterView, DRM or other mechanisms for easy remote access.

Examples of typical products of the global TM system are shown in Figs. 7.1.9-7.1.12. Fig. 7.1.9 shows an example of the structure of a global threshold "snapshot". For illustration purposes, only one station is used rather than a global network (the Apatity array in NW Russia). The color scale gives an indication of the instantaneous thresholds (for a specified origin time) using this station only. It is noted that the threshold is around m_b 4.0 over large parts of the northern hemisphere, increasing toward m_b 5.5 in the shadow zone (epicentral distance 90-110 degrees) and then decreasing to m_b 4.5-5.0 in the PKP zone. Note in particular the threshold increase in a region about 10 degrees from the station. This is due to a local event occurring within a few minutes of the time of the "snapshot", which causes the threshold to increase in the region that would have corresponding P travel times. Also note that the thresholds show a slight variation with azimuth due to the formation of beams and differences in "noise suppression", especially during interfering events.

Figs. 7.1.10 and 7.1.11 are "regional threshold displays", showing sections of the global map (eastern Asia and Africa/Middle East, respectively). On these figures the grid points are especially marked. These two figures illustrate that the variability in threshold at teleseismic distances is sufficiently resolved by the 642-point global grid. There may, however, be a need for a denser grid in cases where stations at local and regional distances are available.

Fig. 7.1.12 is an example of a trace plot corresponding to a selected point on the global grid. This is an example of a site-specific application, although optimized threshold processing is not performed in this case (which is based on the "generic" global map). To

optimize the processing for areas of particular interest, it will be necessary to include detailed calibration information.

Conclusions

The continuous threshold monitoring technique represents a new approach toward achieving reliable seismic monitoring. The method is well suited to supplement the traditional methods in monitoring potential test sites for the purpose of verifying nuclear test ban treaties. The method may equally well be used to monitor earthquake activity at low magnitudes for sites of special interest, and could also be useful for monitoring earthquake aftershock sequences. The prototype system described in this paper is intended to demonstrate how the concept can be used to enable threshold monitoring on a global basis, with applications to real-time displays.

It is important to be aware that the main purpose of the threshold monitoring method is to call attention to any time instance when a given threshold is exceeded. This will enable the analyst to focus his efforts on those events that are truly of interest in a monitoring situation. He will then apply other, traditional analysis tools in detecting, locating and characterizing the source of the disturbance. Thus, the threshold monitoring method is a supplement to, and not a replacement of, traditional methods.

T. Kværna
F. Ringdal
H. Iversen
N.H.K. Larsen

References

Bache, T.C., S.R. Bratt, J. Wang, R.M. Fung, C. Kobryn & J.W. Given (1990): The Intelligent Monitoring System, *Bull. Seism. Soc. Am.*, 80, Special Issue, 1833-1851.

Hannon, W. (1985): Seismic verification of a comprehensive test ban, *Science*, 227, 251-257.

Harjes. H.-P. (1984): Global seismic network assessment for teleseismic detection of underground nuclear explosions, *Tech. Rep. C84-02*, Center for Seismic Studies, Washington, D.C.

Kværna, T. (1991): Initial development of generic relations for regional threshold monitoring, Semiannual Tech. Summ., 1 Apr - 30 Sep 1990, *NORSAR Sci. Rep. 1-90/91*, NORSAR, Kjeller, Norway.

Kværna, T. (1992): Initial results from global Generalized Beamforming, Semiannual Tech. Summ., 1 Apr - 30 Sep 1992, *NORSAR Sci. Rep. 1-92/93*, NORSAR, Kjeller, Norway.

Lilwall, R.C. & P.D. Marshall (1986): Body wave magnitudes and locations of Soviet underground explosions at the Novaya Zemlya test site, *AWRE Rep. NO 017/86*, Blacknest, U.K.

Ringdal, F. (1986): Study of magnitudes, seismicity and earthquake detectability using a global network, *Bull. Seism. Soc. Am.*, 76, 1641-1659.

Ringdal, F. & T. Kværna (1989): A multichannel processing approach to real time network detection, phase association and threshold monitoring, *Bull. Seism. Soc. Am.*, 79, 1927-1940.

Ringdal, F. & T. Kværna (1991): Continuous threshold monitoring using "regional threshold displays", Semiannual Tech. Summ., 1 Oct 90 - 31 Mar 91, *NORSAR Sci. Rep. 2-90/91*, NORSAR, Kjeller, Norway.

Ringdal, F. & T. Kværna (1992): Continuous seismic threshold monitoring, *Geophys. J. Int.*, 111, 505-514.

Sereno, T.J. & S.R. Bratt (1989): Seismic detection capability at NORESS and implications for the detection threshold of a hypothetical network in the Soviet Union, *J. Geophys. Res.*, 94, 10397-10414.

Sykes, L. & J. Evernden (1982): The verification of a comprehensive nuclear test ban, *Sci. Am.*, 247, 47-55.

Vinje, V., E. Iversen, H. Gjøystdal & K. Åstebøl (1992): Traveltime and amplitude estimation using wavefront construction. Abstract of paper presented at the 54th Meeting and Technical Exhibition of the European Association of Exploration Geophysicists, Paris, France, 1-5 June 1992.

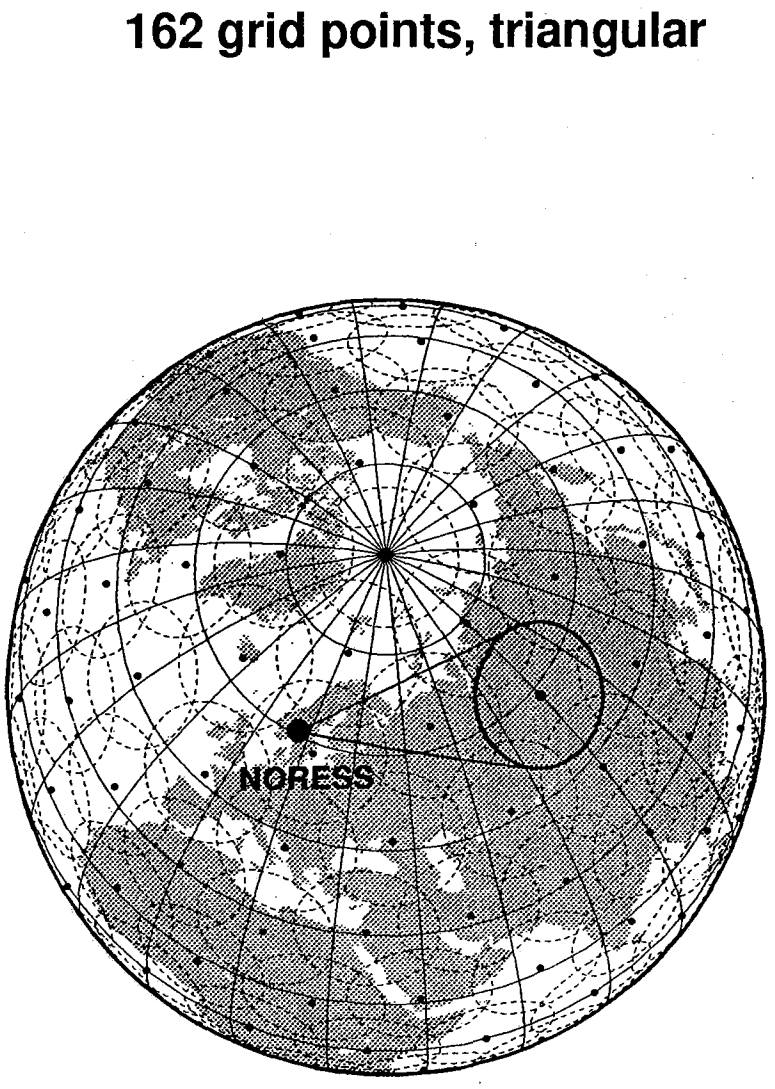

Fig. 7.1.1. A 162-point global grid system projected onto an azimuthal orthographic projection of the earth. The circular target regions are shown by dashed circles, and the highlighted target region is used as an example of time and azimuth tolerances in this study. Its center point is located 37.5 degrees from the NORESS array. Minimum and maximum azimuthal lines from NORESS to the target region are also shown.

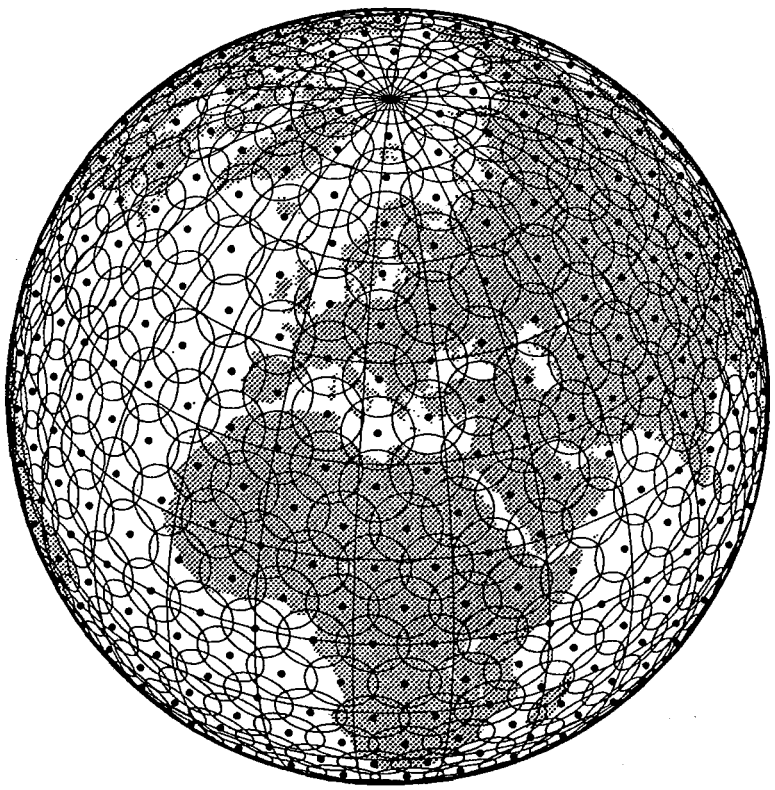

Fig. 7.1.2. Circular regions of radius 5.5 deg encompassing each grid point constructed by the triangular method. Note that the coverage is complete.

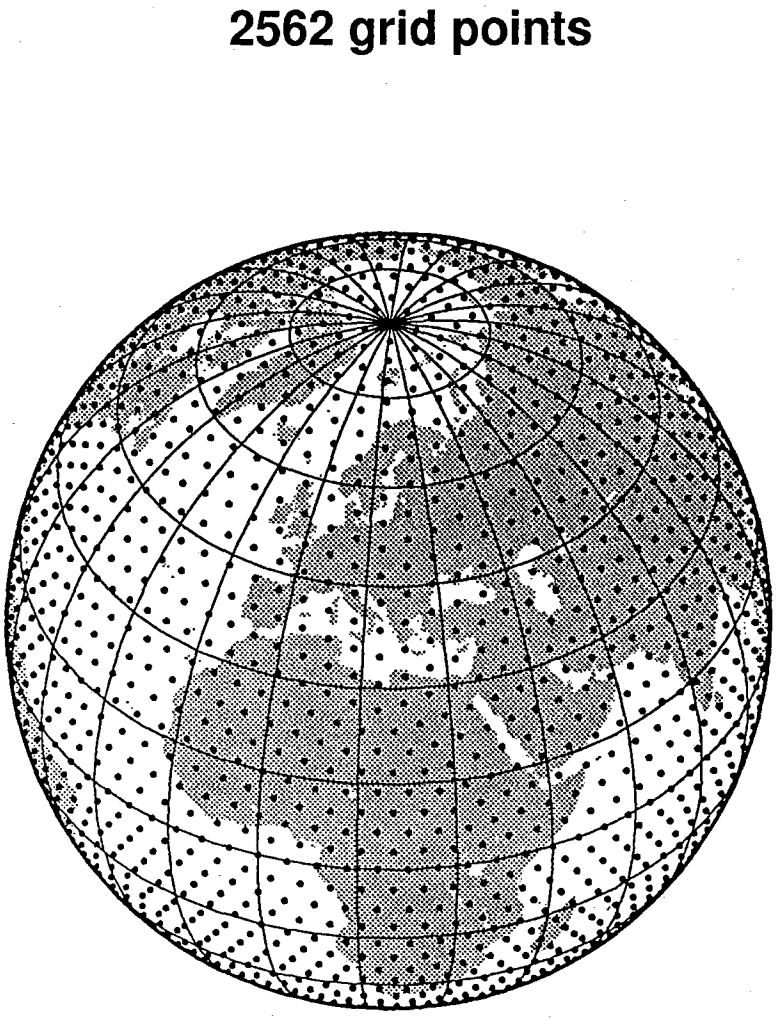

Fig. 7.1.3. A 2562-point global grid system projected onto an azimuthal orthographic projection of the earth. This grid system was obtained by a four-fold triangulation of the icosaeder, and each grid point represents a target region of 2.7 degrees radius.

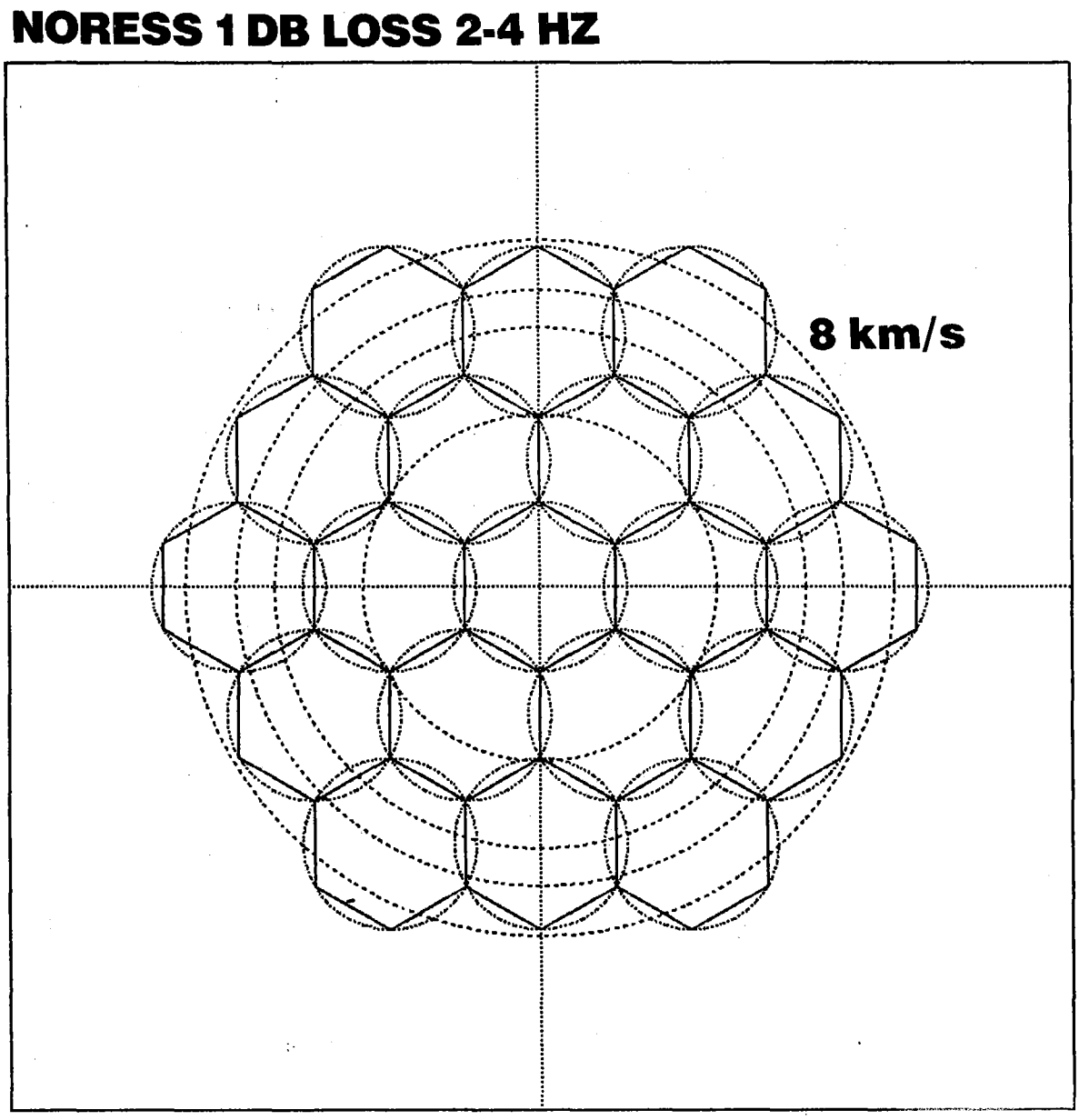

Fig. 7.1.4. Example of NORESS beam pattern, displayed in inverse velocity space, corresponding to a deployment with a worst-case beam-steering loss of 1 dB (filter band 2-4 Hz). The figure covers typical P-wave velocities for regional and teleseismic distances (8 km/s and up).

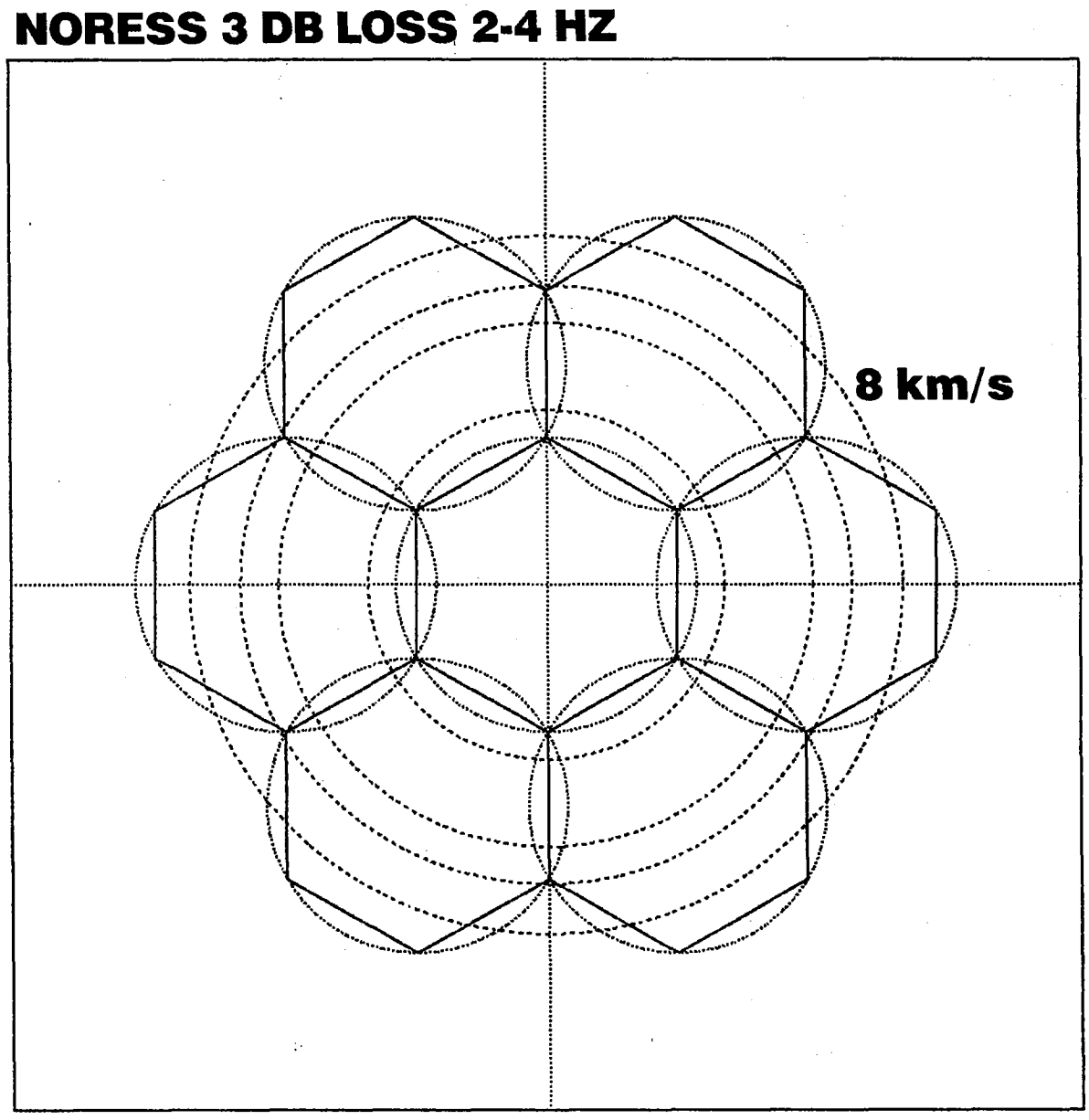

Fig. 7.1.5. Same as Fig. 7.1.4, but allowing a worst-case beam-steering loss of 3 dB. Note that the number of beams required is significantly lower than for the 1 dB loss case (7 vs 19).

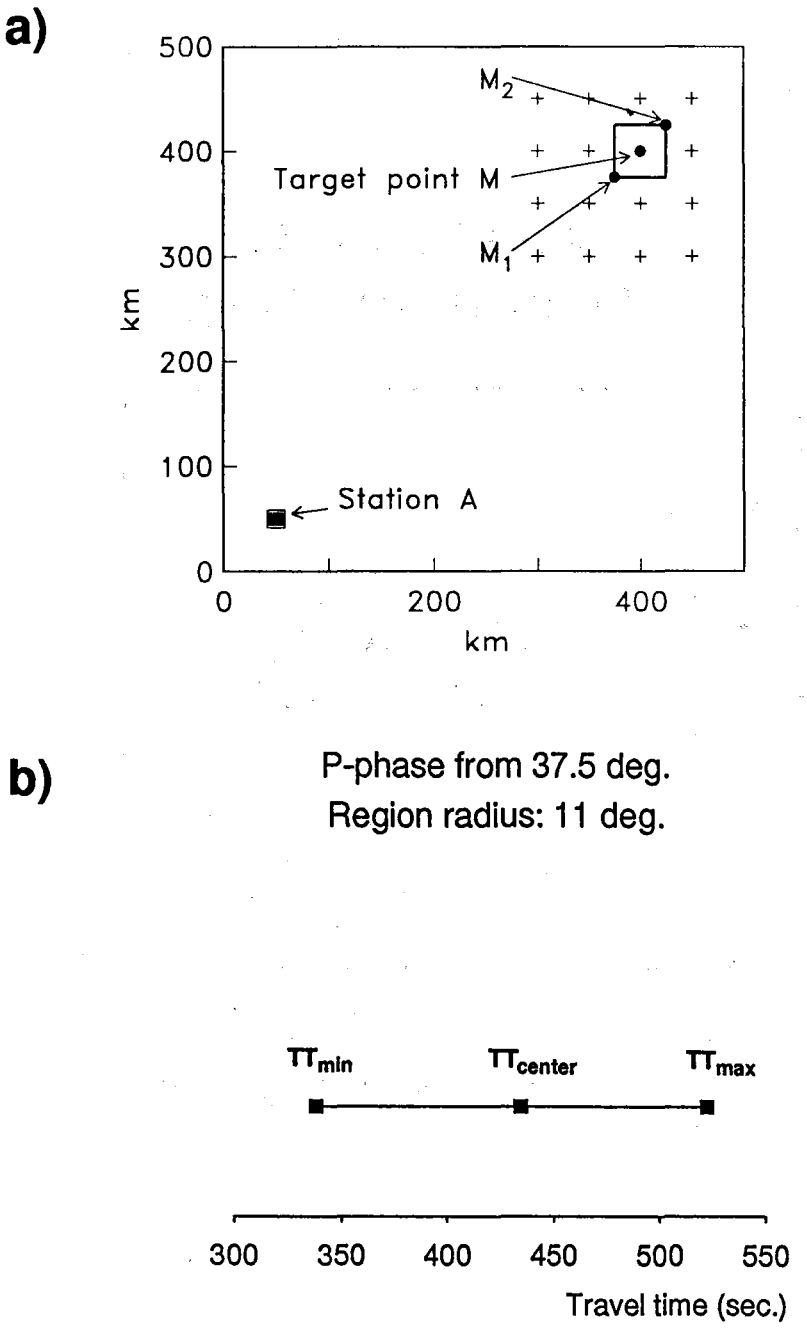

Fig. 7.1.6. The *top part* of this figure illustrates the necessity of using time tolerances when using one target point to represent an area. The plus signs indicate target points, and a rectangle surrounding one of the target points (M) is also given. The point within the rectangle with the minimum traveltime is denoted M_1, whereas the point with the maximum traveltime is denoted M_2. The *bottom part* of the figure shows the range of predicted P-wave travel times from the highlighted target region of Fig. 7.1.1 to the NORESS array.

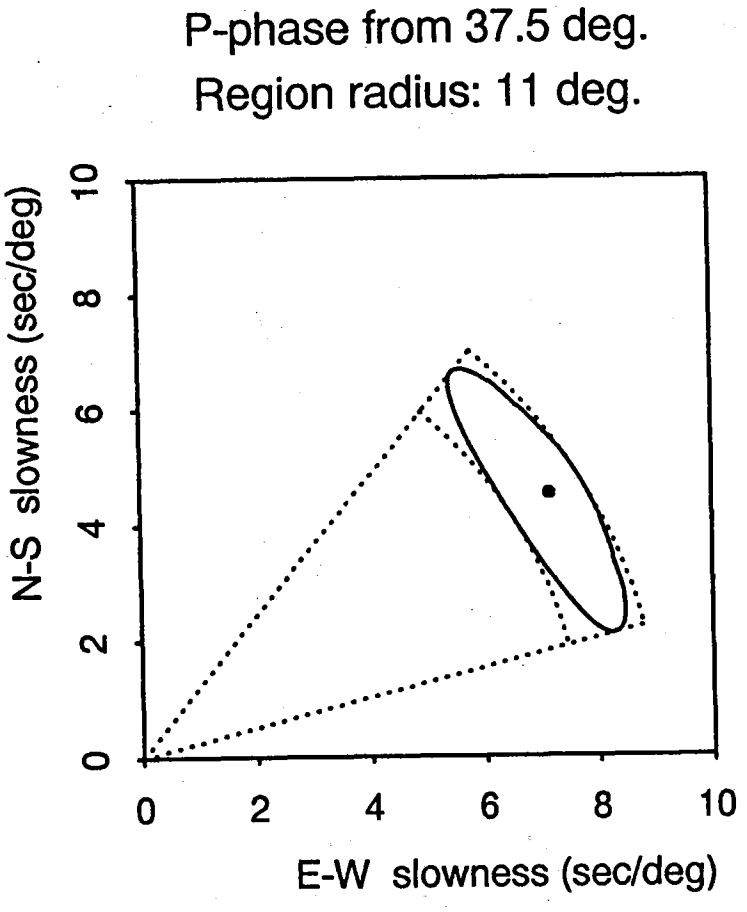

Fig. 7.1.7. In order to monitor a finite area surrounding each of the target points, a mis-steering in azimuth is introduced when the beams are steered towards the target points. This figure illustrates the range of predicted P-wave slowness vectors at NORESS for events in the highlighted target region of Fig. 7.1.1. The slowness vectors of the circular boundary of the target region are projected onto the solid line of this figure. An approximation to the area inside this solid line is given by the dotted sector segment defined by the minimum and maximum azimuths and the minimum and maximum slownesses.

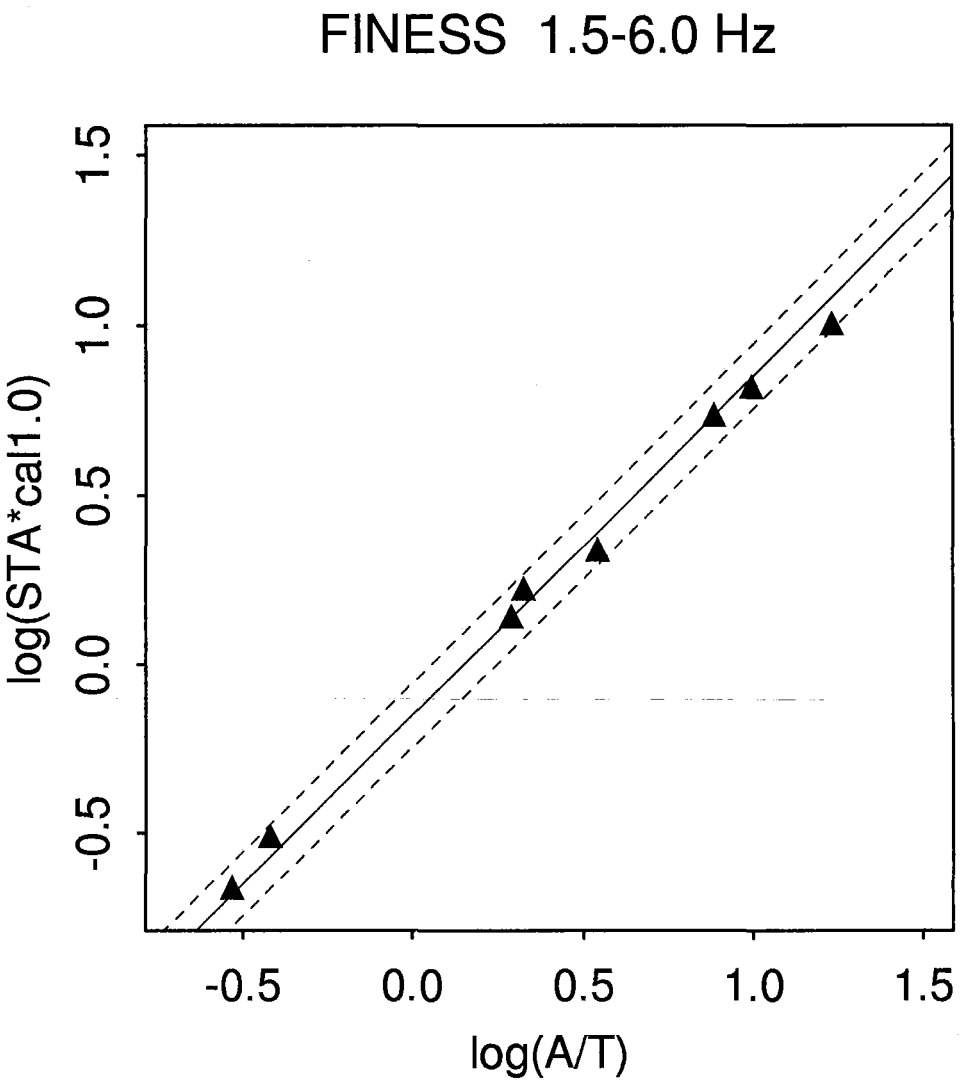

Fig. 7.1.8. Figure illustrating the linear dependency between log (A/T) and log (STA x cal). For the station FINESS and the frequency band 1.5-6.0 Hz, shown on the figure, the best-fitting straight line (with a restricted slope of 1.0) is:

$$\log (STA \times cal) = \log (A/T) - 0.15$$

Thus, in this case the constant c in formula (2) is 0.15.

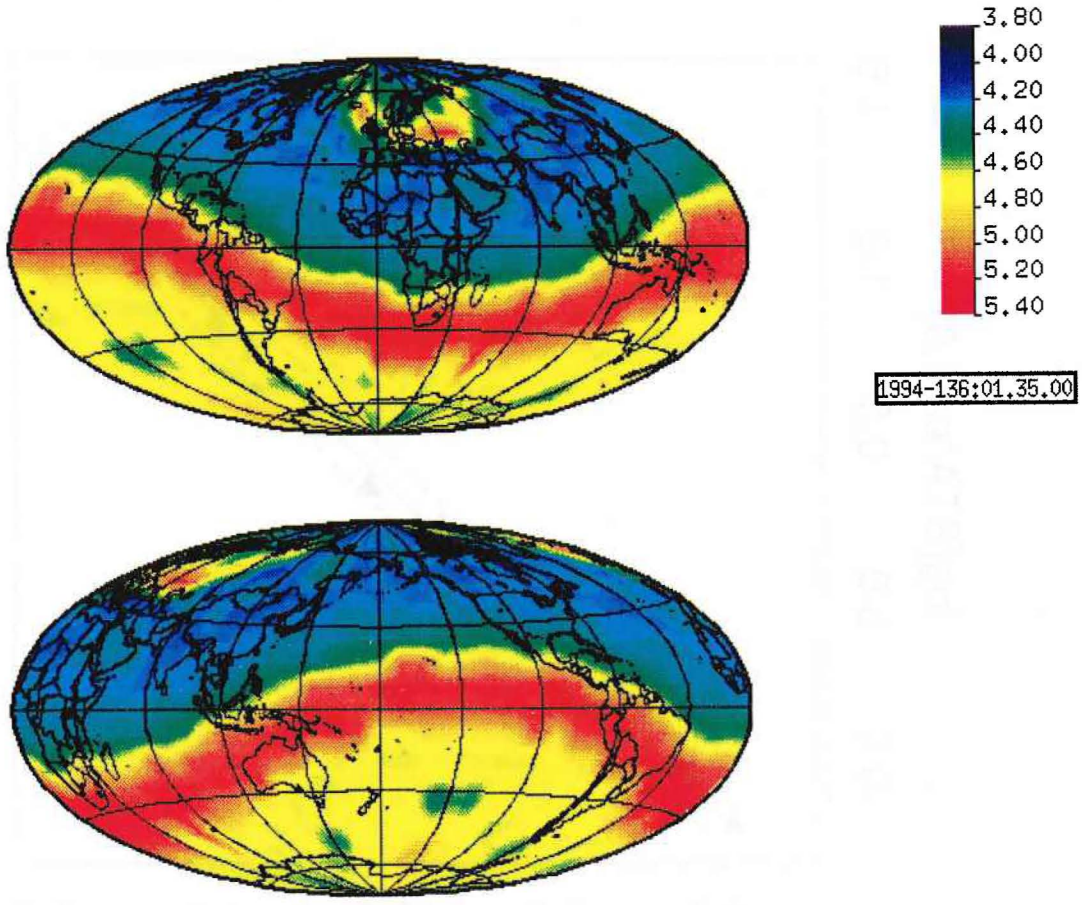

Fig. 7.1.9. Illustration of global threshold monitoring for the simplified case of a monitoring "network" consisting of one array (the Apatity station in NW Russia). The figure shows instantaneous thresholds globally (with two different world map perspectives) for a specified origin time. As illustrated by the color coding, the threshold ranges from near 4.0 in much of the northern hemisphere to about 5.5 in the shadow zone. Note the effect of a preceding local event on the threshold near Scandinavia (see text for details).

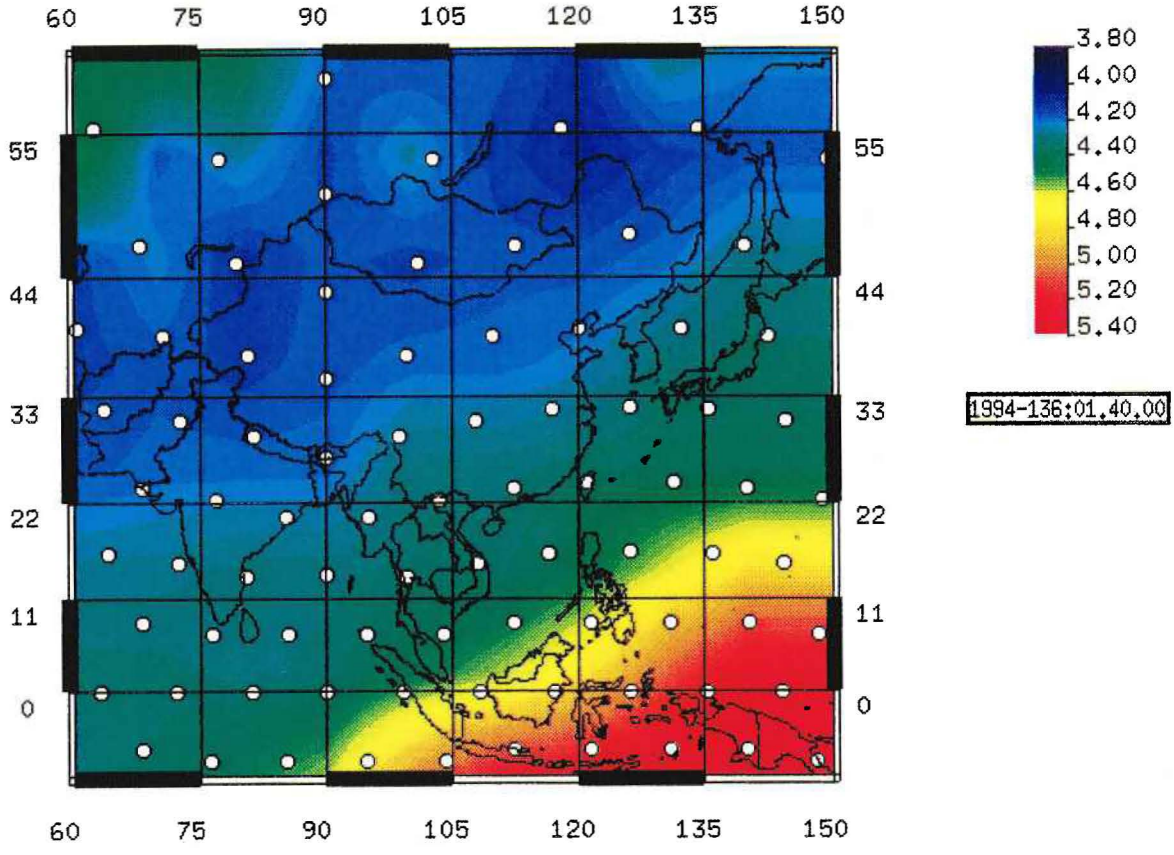

Fig. 7.1.10. A regional threshold map excerpted from the global map of Fig. 7.1.9. The figure shows the eastern Asia region, and grid points corresponding to the global 642 points triangularization (Fig. 7.1.2) are especially marked.

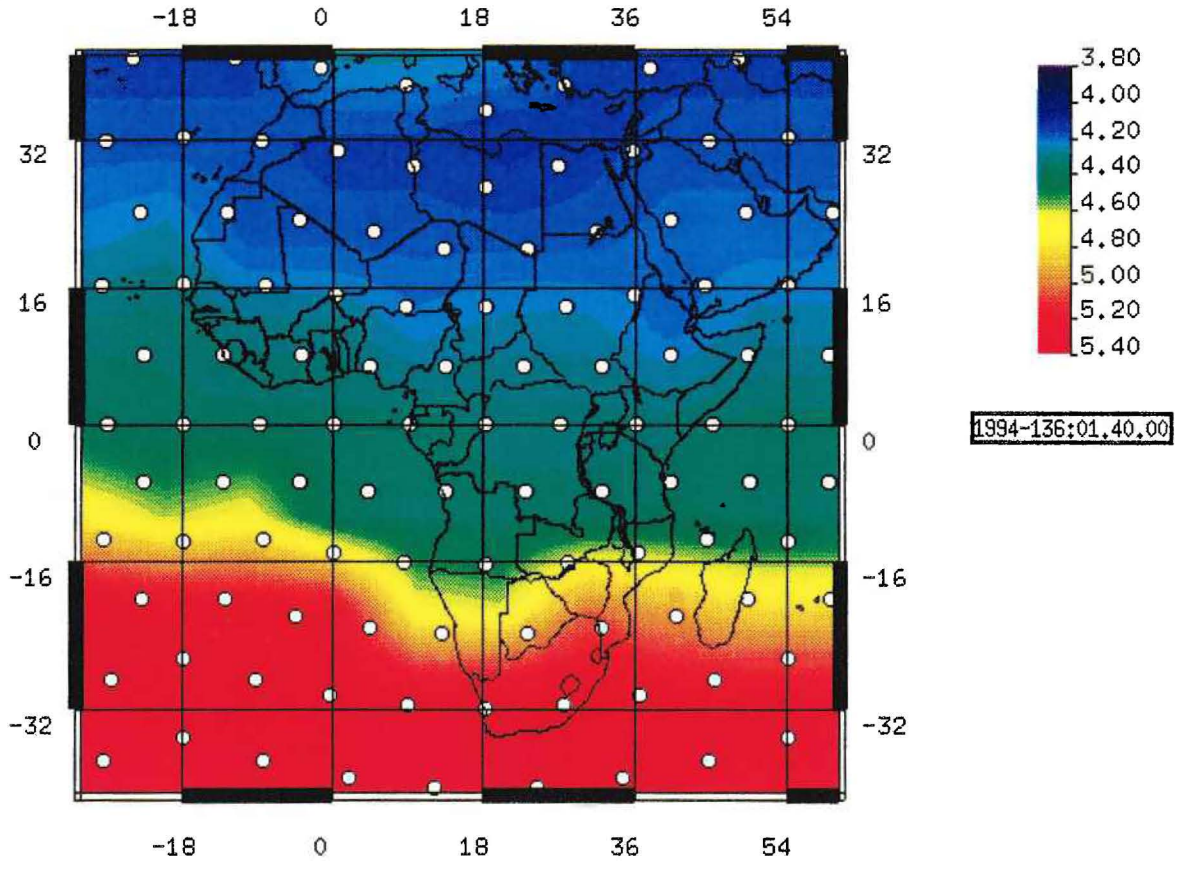

Fig. 7.1.11. Similar to Fig. 7.1.10, but covering the region of Africa/Middle East.

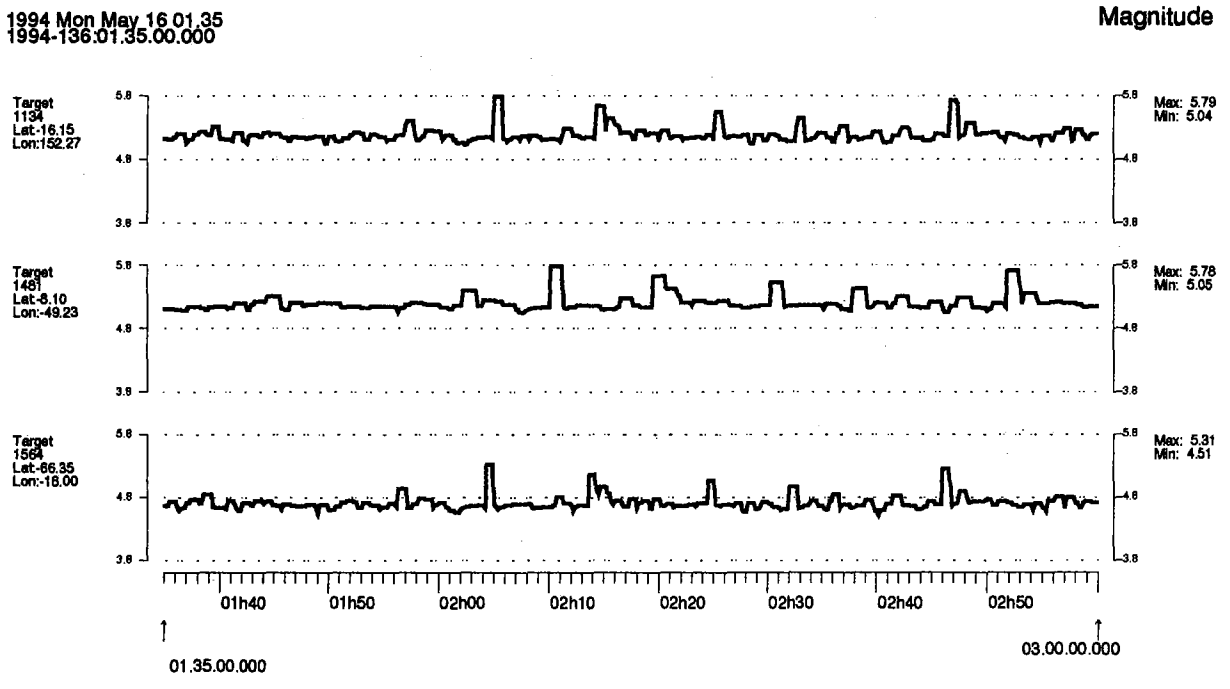

Fig. 7.1.12. Figure illustrating the display of individual threshold traces as a function of time. Traces corresponding to three grid points on the global map (all at teleseismic distances) are shown. Each trace covers about 1 1/2 hours. Such traces can be displayed interactively by clicking on the points of a global or regional map (Figs. 7.1.9-7.1.11) and specifying the desired time interval. This example is based on only one station in the "network" (the Apatity array).